Hindawi
Journal of Sensors
Volume 2018, Article ID 8017614, 12 pages
https://doi.org/10.1155/2018/8017614

Research Article

Application of Fractional Differential Calculation in Pretreatment of Saline Soil Hyperspectral Reflectance Data

Anhong Tian,[1,2] Junsan Zhao,[1] Heigang Xiong,[3,4] Shu Gan,[1] and Chengbiao Fu[1,2]

[1]*Faculty of Land Resource Engineering, Kunming University of Science and Technology, Kunming, Yunnan 650093, China*
[2]*College of Information Engineering, Qujing Normal University, Qujing, Yunnan 655011, China*
[3]*College of Applied Arts and Science, Beijing Union University, Beijing 100083, China*
[4]*College of Resource and Environment Sciences, Xinjiang University, Urumqi, Xinjiang 830046, China*

Correspondence should be addressed to Junsan Zhao; jszht@kmust.edu.cn

Received 22 May 2018; Revised 17 August 2018; Accepted 2 September 2018; Published 11 October 2018

Guest Editor: Christine Pohl

Pretreatment of spectrum data is a necessary and effective method for improving the accuracy of hyperspectral model building. Traditional differential calculation pretreatment only considers the integer-order differential, such as the 1st order and 2nd order, and overlooks important spectrum information located at fractional order. Since fractional differential (FD) has rarely been applied to spectrum field measurement, there are few reports on the spectrum features of saline soils under different degrees of human interference. We used FD to analyze field spectrum data of saline soil collected from Xinjiang's Fukang City. Order interval of 0.2 was adopted to divide 0–2 orders into 11-order differentials. MATLAB programming was used to convert the raw spectral reflectance and its four common types of mathematics and to conduct FD calculation. Spectrum data for area A (no human interference area) and area B (human interference area) was separately processed. From the statistical analysis of soil salinization characteristics, the salinization degree and type for area B were more diverse and complicated than area A. MATLAB simulation results showed that FD calculation could depict the minute differences between different FD order spectra under different human interference areas. The overall differential value trend appeared to move towards 0 reflectance value. After differential processing, the trend of bands that passed the 0.05 significance test of correlation coefficient (CC) showed an increase first then decrease later. The maximum CC absolute value for five spectrum transformations all appeared in the fractional order. FD calculation could significantly increase the correlation between spectral reflectance and soil salt content both for full-band and single-band spectra. Results of this study can serve as a reference for the application of FD in field hyperspectral monitoring of soil salinization for different human interference areas.

1. Introduction

Pretreatment of spectrum data is a very effective way of increasing the precision of hyperspectral model building. Spectrum differential (derivative) technology is a very valuable analytical method in hyperspectral data pretreatment that is often applied to increasing the strength of spectrum signals [1], which can quickly determine the inflection point and maximum and minimum reflectivity band positions. Studies have shown that the first-order differential can eliminate the influence of a partially linear or near-linear noise spectrum on the target spectrum [2]. The second-order differential can effectively eliminate the baseline drift and background signal and improve the pretreatment accuracy [3]. However, in the study of monitoring soil salinization by hyperspectral techniques, most of the spectral data are preprocessed based on the integer-order (1st order or 2nd order) differential algorithm to enhance the correlation between partial bands' reflectivity and surface parameters. But some studies have pointed out that the spectral reflectance curve of the first-order and second-order differential transformation differs greatly from the original spectral reflectance curve [4]. Only considering the integer-order differential transformation ignores the important spectral information located in the fractional order, resulting in a problem of reduced modeling accuracy. At the same time, many systems

in reality belong to the fractional order. When the model is expressed by integer differential, the accuracy is not ideal.

At present, FD has a small amount of research in the field of spectral analysis. FD was first used in diffuse reflectance spectroscopy. In recent years, FD has been used in public datasets such as diesel, corn, and wheat, as well as to analyze the spectral pretreatment effects of Xinjiang's saline soil in laboratory environments. For example, Schmitt [5] used fractional differentiation to process the diffuse-reflectance spectra; simulations revealed that fractional derivative spectroscopy separated the overlapping peaks between spectra and deleted baseline variations. Also, due to the features of memory and nonlocality of FD, it was allowed to control the sensitivity to the slope and curvature of spectrum curve according to the weight of different differential orders; this offered more range for band selection in regression modeling. Kharintsev and Salakhov [6] adopted the FD method to acquire the spectrum parameters for overlapping wavelength bands, in order to overcome the high variance features of spectrum parameters for the tradition ordinary least squares method. Also, a statistical regularization method is used to determine the stable and unbiased estimation for fractional differentiation and the overlapping wavelength bands identified by a Tsallis distribution model. Results showed that fractional derivatives could be effectively used in the field of spectral analysis. Zheng et al. [7] proposed a fractional-order Savitzky-Golay differentiation (FOSGD) method on the basis of Riemann-Liouville (R-L) fractional calculus theory; it was used to preprocess the near-infrared (NIR) spectrum datasets for corn data, diesel data, and wheat data. FOSGD could increase the model performance for least squares regression, and the root mean square error (RMSE) was smaller than integral differential, especially for the nonconcentration indexes such as viscosity, density, and hardness. In the field of soil spectral analysis, Zhang et al. [8] first used the FD algorithm to preprocess soil spectral data in the laboratory. Zhang et al. collected the saline soils in Yutian Oasis of Xinjiang, China, and analyzed the correlation between soil salinity and spectra by a Grünwald-Letnikov (G-L) FD algorithm. Simulation showed that the G-L algorithm enriched the preprocessing method of hyperspectral data from the perspective of fractional order. The depth of the deep mining of the potential information in the spectral data could greatly raise the correlation between salt content and the spectra and the CC obtained at the fractional order instead of the traditional integer order (1^{st} order, 2^{nd} order). Also, this novel pretreatment method for saline soils could prevent the loss of important information caused by only considering the traditional integer order. Xia et al. [9] took the 43 saline soil samples of Ebinur Lake in Xinjiang, China, as data sources, and analyzed the correlation between original spectral reflectance and electrical conductivity. Results showed that fractional derivate could improve the CC for some single bands, such as 505 nm, 2239 nm, and 2443 nm. Also, it could detail the change trends between integer and fractional curve.

In addition, the type of human activities, level, and the duration has an important impact on soil feature and heterogeneity [10]. The changes of regional salt are not only deeply affected by global warming but also by the interaction of regional environmental elements and human activities [11]. The impact of human activities on the soil is conscious and purposeful. The influence of human activities on soil development can be in two ways, that is, the soil can be developed in a direction of benign circulation through rational use of soil and soil degradation can be caused by irrational use. Therefore, different degrees of human activities will inevitably lead to differences in regional soil morphological characteristics (structure, texture, tightness, porosity, dry humidity, etc.), triggering changes in salt transfer channels and salt transmit rates and thus increasing the complexity of salt spatial variability of soil salinity. As a result, the time-space dynamics of the oasis salt and the changes in the ecological environment are also very different. Therefore, the relationship between land use change and soil salinization is the focus of current attention. Soil salinization is an important environmental problem in the arid and semiarid areas of Xinjiang [12, 13]. Soil salinization causes decreased fertility, pH imbalance, and degradation of the land, which severely restricts the development of China's agricultural economy [13, 14]. Because hyperspectral remote sensing technology has many spectrum reflectance bands, has high spectral resolution, and does not damage the testing sample [15–18], it has been widely used in hyperspectral data study on saline soil under human interference [19, 20]. However, hyperspectral remote sensing has been rarely used in study on correlation between saline soil features under different levels of human interference and their spectrum features.

However, these aforementioned soil studies are focused on soils under human interference and the soil spectrum reflectance value was obtained in ideal indoor environment; the solar light source was simulated by a halogen lamp, without considering the influence of actual environmental factors in the field, and the inversion model established by indoor spectra may not be directly applicable to field remote sensing inversion. Therefore, the construction of soil physical and chemical properties' inversion model based on field spectroscopy is necessary. Field spectral measurements use the sun as a source of light to ensure equivalence with remote sensing image acquisition [21]. Currently FD has rarely been reported to field spectrum measurement. Thus, we used saline soil from areas with and without human interference in Xinjiang's Fukang City as the subject to explore the pretreatment effect of FD for field spectrum measurements. MATLAB R2015a software was used for FD calculation. Spectrum data from area A (no human interference) and area B (with human interference) were processed. For the order interval, 0.2 was used. The raw spectrum and the four types of transformation were put through 0–2^{nd}-order differential processing with a total of 11 orders. The application prospects of the FD algorithm in the pretreatment of field measured spectra under different human interference levels are discussed, which provides a new idea for studying the temporal and spatial variations of salt in oasis in the arid regions.

2. Study Area and Data

2.1. Study Area. The study area is located between the southern edge of Dzungarian Basin and the Northern Foothill of

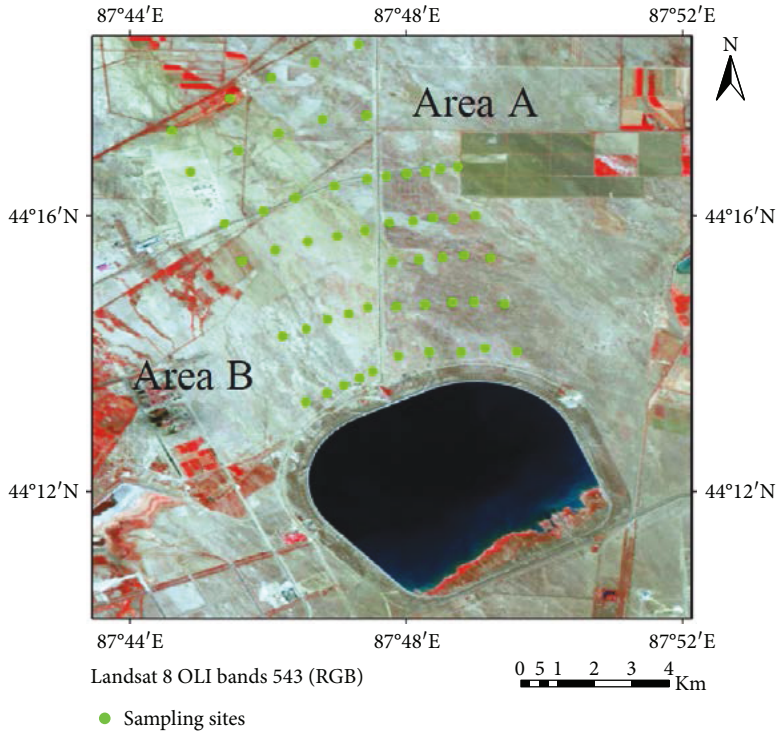

Figure 1: Location of the study area and the distribution of soil samples.

(a) (b)

Figure 2: Sampling environment for area A: (a) one, (b) two.

Xinjiang's Tianshan Mountain (87°44′–88°46′E, 43°29′–45°45′N). This area has temperate continental climate. Thus, this area has hot summers and cold winters, and the day and night temperatures differ significantly. This area has ample light and heat, and the annual average temperature is 6.7°C. However, this area has little rainfall, and the annual rainfall is around 164 mm. Five east-west running sampling lines with a 600–800-meter gap in between were established in area A (starting from the northern part of area A to the southern part of area A). Six sampling lines with a 800–1000-meter gap were established in area B. Five representative sampling points were selected for each sampling line. The intervals between the sampling points were 300–500 meters. GPS positioning was implemented for the 55 sampling points, as shown in Figure 1. Overall, 25 sampling points were used for area A and 30 sampling points were used for area B.

2.2. Division of Areas with Different Interference Levels. The sampling area is the alluvial fan edge located southeast of Xinjiang's Fukang City 102 Army Corp. There is a north-south travelling canal laid with impermeable membrane in the center of this area that is 24 m wide on top, 6 m wide on the bottom, 5 m deep, and 15.30 km long. Thus, we used this canal as the boundary to divide the research area into areas A and B for sampling. Area A is located further away from human habitat and is segregated by the canal; therefore, it is not affected by human activity. The soil is an alkali soil with sparse Haloxylon ammodendron, Tamarix ramosissima, and Ceratocarpus arenarius growth, as shown in Figure 2. Testing showed that the soil salinization was more severe and the pH value was approximately 7.76–8.98. The salt content of the top layer [10] was 5.34–44.45 g/kg.

Area B is near the 102 Army Corp and experiences strong human activities. The land has mostly been developed, and

(a) (b)

Figure 3: Sampling environment for area B: (a) one, (b) two.

the development method is primarily artificial Haloxylon ammodendron woodland, seedling cultivation land, and elm woods, as shown in Figure 3. Because area B is regular woodland, it has only been tilled but does not have fertilizer added. Therefore, the research area has been divided into two categories based on the threat level of human activities on the oasis ecological environment, area A with no human interference and area B with human interference.

2.3. Soil Sample Collection and Field Spectrum Measurement. The sample collection time was in the middle of May in 2017. A portable FieldSpec® 3 Hi-Res spectrum spectrometer produced by American ASD Corporation was used to obtain spectrum data from the soil test. The spectrum effective range for this instrument is 350–2500 nm. The spectrum sampling interval is 1.4 nm for the 350–1000 nm range and 2 nm for the 1000–2500 nm range. The resampling interval is 1 nm. ASD ViewSpec Pro was used as the analysis software. Because weather conditions can affect spectrum testing, the spectrum test for this study was conducted between 11:00 and 15:00 hours local time to reduce data error caused by weather factors. The spectrum test was conducted during times when the sky was clear with no cloud and no wind. Before each spectrum test, the spectrum spectrometer was conducted on the whiteboard calibration to remove effects from dark current. The probe of the spectrum spectrometer was placed 15 cm directly above the sampling surface to collect the spectrum. To prevent surface cracks and surrounding plants from affecting the soil spectrum test, each spectrum test sampling point was chosen to be away from items that can interfere with the soil spectrum. Spectrum from five locations within 1 meter of the sampling point with a similar soil background value was collected. Each point was tested 10 times to obtain 10 spectrum curves, with a result of 50 curves for each sampling location. The mean of these spectrum tests was used as the actual tested spectrum value for each sampling point.

While conducting the spectrum field measurement, 0–20 cm of the soil sample was collected from each sampling point and placed in a numbered bag. Once taken back to the laboratory, the samples were air dried naturally and had impurities removed. After sieving through 1 mm holes, the samples were sent to the Xinjiang Institute of Ecology and Geography (Chinese Academy of Sciences) to test the soil salt content by professional personnel.

2.4. Spectrum Data Analysis. At first, to reduce the effect from noise, peripheral bands from 350 to 399 nm and 2401 to 2500 nm with lower signal noise were removed. Bands in the moisture absorption segment (1355–1410 nm and 1820–1942 nm) were also removed. Moreover, Savitzky-Golay filtering was then used to conduct spectrum smoothing to remove noise. At last, to reduce the effects of atmospheric background noise, four different types of mathematical transformations are used for the raw spectral reflectance (R), that is, root mean square ($\sqrt{R}$) transformation, reciprocal ($1/R$) transformation, logarithmic reciprocal ($1/\log R$) transformation, and logarithm ($\log R$) transformation.

3. Methodology

3.1. Comparison of Fractional Differential and Integer Differential. According to the theoretical knowledge of integer-order calculus, the function $f(x)$ has n-order continuous derivative characteristics and h is an increment. The first-order, second-order, and third-order derivatives of function $f(x)$ can be expressed as

$$f'(x) = \frac{df}{dx} = \lim_{h\to 0}\frac{f(x)-f(x-h)}{h},$$
$$f''(x) = \left(\frac{df}{dx}\right)' = \lim_{h\to 0}\frac{f(x)-2f(x-h)+f(x-2h)}{h^2},$$
$$f'''(x) = \frac{d^3f}{dx^3} = \lim_{h\to 0}\frac{f(x)-3f(x-h)+3f(x-2h)-3f(x-3h)}{h^3}. \quad (1)$$

FD has been successfully applied to system model building, signal filter, pattern recognition, and fractal theory [22–24]. This is mainly because in these applications, the fractional-order model has more accurate results than the original integer differential model. FD mainly has three forms of expressions [8, 9]: Riemann-Liouville (R-L), Grünwald-

Table 1: Salinization degree and soil sample classification statistics.

Salinization degree	Salt content (g/kg)	Area A			Area B		
		Samples	Proportion (%)	Mean (g/kg)	Samples	Proportion (%)	Mean (g/kg)
Nonsaline soil	<3.0	0	0.000%	0	1	3.333%	2.700
Mild saline soil	3.0~5.0	0	0.000%	0	2	6.667%	3.775
Moderate saline soil	5.0~10.0	1	4.000%	7.150	6	20.000%	7.358
Severe saline soil	10.0~20.0	21	84.000%	15.220	13	43.333%	15.519
Saline soil	>20.0	3	12.000%	26.475	8	26.667%	25.678

Table 2: Classification criteria of the soil salinization type and soil sample classification statistics.

$C(Cl^-)/2C(SO_4^{2-})$	Salinization type	Zone A		Zone B	
		Samples	Proportion (%)	Samples	Proportion (%)
<0.20	SO_4^{2-} salt type	22	88.000%	14	46.667%
0.20–1.00	Cl^--SO_4 salt type	3	12.000%	12	40.000%
1.00–2.00	SO_4-Cl^- salt type	0	0	3	10.000%
>2.00	Cl^- salt type	0	0	1	3.333%

Note: $C(Cl^-)$ and $C(SO_4^{2-})$, respectively, represent the millimole amount of Cl^- and SO_4^{2-} contained in 100 g soil.

Letnikov (G-L), and Caputo. Of which, the generally G-L FD can be defined as

$$d^{\alpha}f(x) = \lim_{h\to 0}\frac{1}{h^{\alpha}}\sum_{m-0}^{(t-a/h)}(-1)^{m} \cdot \frac{\Gamma(\alpha+1)}{m!\Gamma(\alpha-m+1)}f(x-mh), \tag{2}$$

where α is the order, h is the differential step size, and t and a are the upper and lower limits of the differential, respectively. Gamma function $\Gamma(z) = \int_0^{\infty} e^{-u}u^{z-1}du = (z-1)!$.

Set one variable function $f(x)$ to define domain $x \in [a, t]$ so that $h = 1$ (this is consistent with the 1 nm sampling interval of the spectrum instrument used for this study). $n = [t-a]$, then (2) can be used to derive the FD difference expression of function $f(x)$:

$$\frac{d^{v}f(x)}{dx^{v}} \approx f(x) + (-v)f(x-1) + \frac{(-v)(-v+1)}{2}f(x-2) + \cdots + \frac{\Gamma(-v+1)}{n!\Gamma(-v+n+1)}f(x-n), \tag{3}$$

where v is the order, the 0 order of function $f(x)$ is $f(x)$ itself. When $v = 1$ and 2, (3) is consistent with the 1st-order differential and 2nd-order differential formula when differential window size $\omega = 1$. In this study, the 0-order differential mathematical transformation refers to the transformation itself and does not undergo differential processing.

It can be seen from (3) that the FD has the features of memory and nonlocality; it is allowed to control the sensitivity to the slope and curvature of spectrum curve according to the weight of different differential orders, and this offers more range for band selection.

3.2. Correlation Coefficient Model Validation Index. CC is adopted to measure the linear correlation between two variables X and Y; its calculation formula can be described as [25–27]

$$CC_{XY} = \frac{\sum_{i=1}^{n}(X_i - \bar{X})(Y_i - \bar{Y})}{\sqrt{\sum_{i=1}^{n}(X_i - \bar{X})^2 \cdot \sum_{i=1}^{n}(Y_i - \bar{Y})^2}}, \tag{4}$$

where $\bar{X}$ and $\bar{Y}$ are, respectively, the average of X_i, and Y_i. CC_{XY} is in the range of −1 to +1. If the value of $|CC_{XY}|$ is closer to 1, it means that the linear relationship between X and Y is higher. In general, when CC_{XY} is higher than 0.8, X variable and Y variable can be regarded as highly relevant. When CC_{XY} is between 0.5 and 0.8, X variable and Y variable can be seen as moderately related. When CC_{XY} is between 0.3 and 0.5, these two variables can be considered as low correlation. When CC_{XY} is lower than 0.3, it means that the correlation between two variables is very weak and can be regarded as nonlinear correlation.

4. Results and Discussion

4.1. Analysis of Soil Salinity Characteristics for Different Interference Areas. According to the soil salt content [28], the degree of salinization was divided into nonsaline soil, mild saline soil, moderate saline soil, severe saline soil, and saline soil (Table 1). Area A was basically heavy saline soil, accounting for 84% of the total sample. Area B was affected by human activities, and the degree of salinization was more diverse, mainly heavy saline soil, saline soil, and moderate saline soil, accounting for 43.333%, 26.667%, and 20% of the total samples, respectively.

In view of the classification of the soil salinization type [28], the salinization type was divided into SO_4^{2-} salt type, Cl^--SO_4 salt type, SO_4-Cl^- salt type, and Cl^- salt type (Table 2). Zone A contained only the SO_4^{2-} and Cl^--

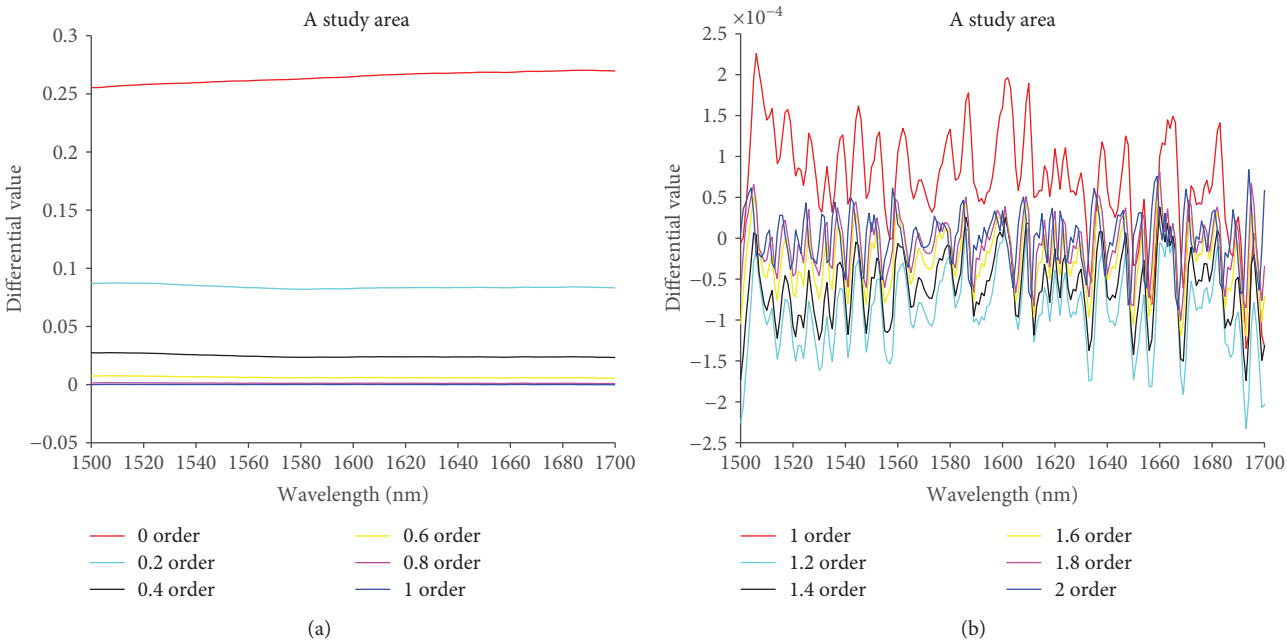

Figure 4: Wavelength 1500–1700 reflectance FD value in area A. (a) 0–1 orders. (b) 1–2 orders.

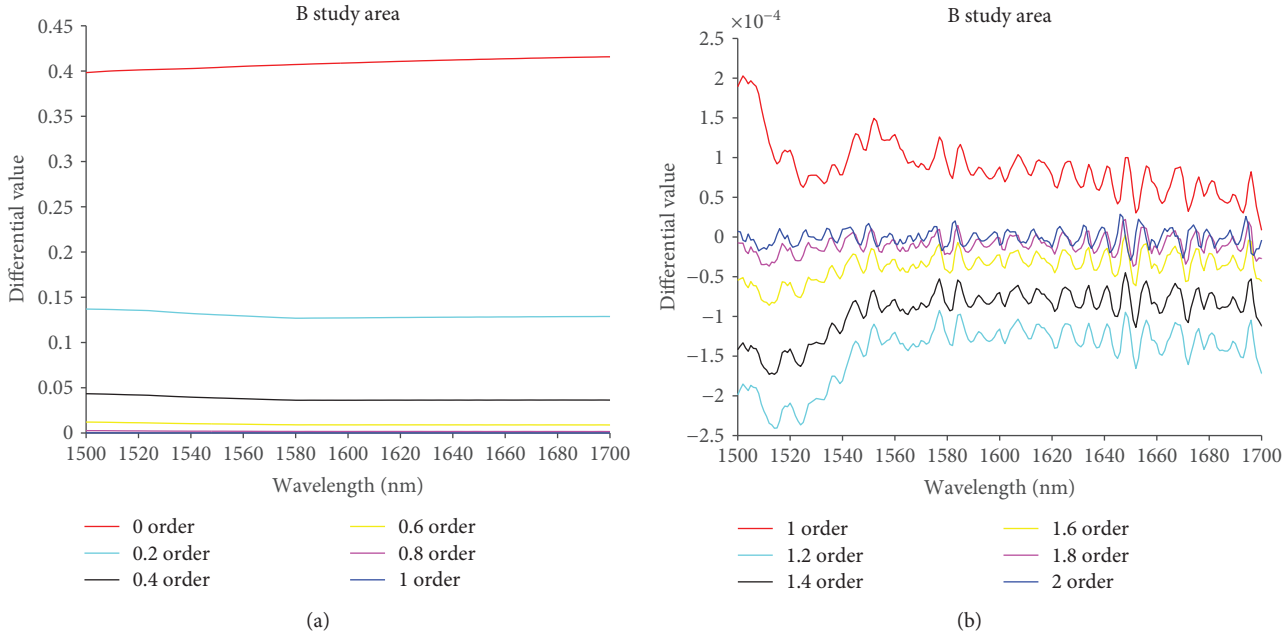

Figure 5: Wavelength 1500–1700 reflectance FD value in area B. (a) 0–1 orders. (b) 1–2 orders.

SO_4 salt types. The soil in zone B contained all four types of salinization.

4.2. FD Simulation Results for Different Interference Areas. Based on the aforementioned formula derivation, the MATLAB R2015a was used for FD calculation and to process the spectrum data from area A and area B. The raw spectrum and the four types of transformation were put through 0–2nd-order differential processing with a total of 11 orders. Using the mean of the raw spectrum from areas A and B as an example, 11-order differential result was shown in Figures 4 and 5. The *X* axis was the wavelength, and the *Y* axis showed the reflectance value of each order after differential processing. Because there were too many bands, simulation result from 1500 to 1700 band was used for comparison purposes. Figures 4 and 5 showed that the overall differential value trend moved towards the reflectance value of 0. The change from 0 order to 1st order was the most obvious. The reflectance value of area A decreased from 0.25 at 0 order to 0.02 at 1st order. The reflectance value of area B decreased from 0.4 at 0 order to 0.02 at 1st order. This showed that the change in differential curve from 0 order to 1st order

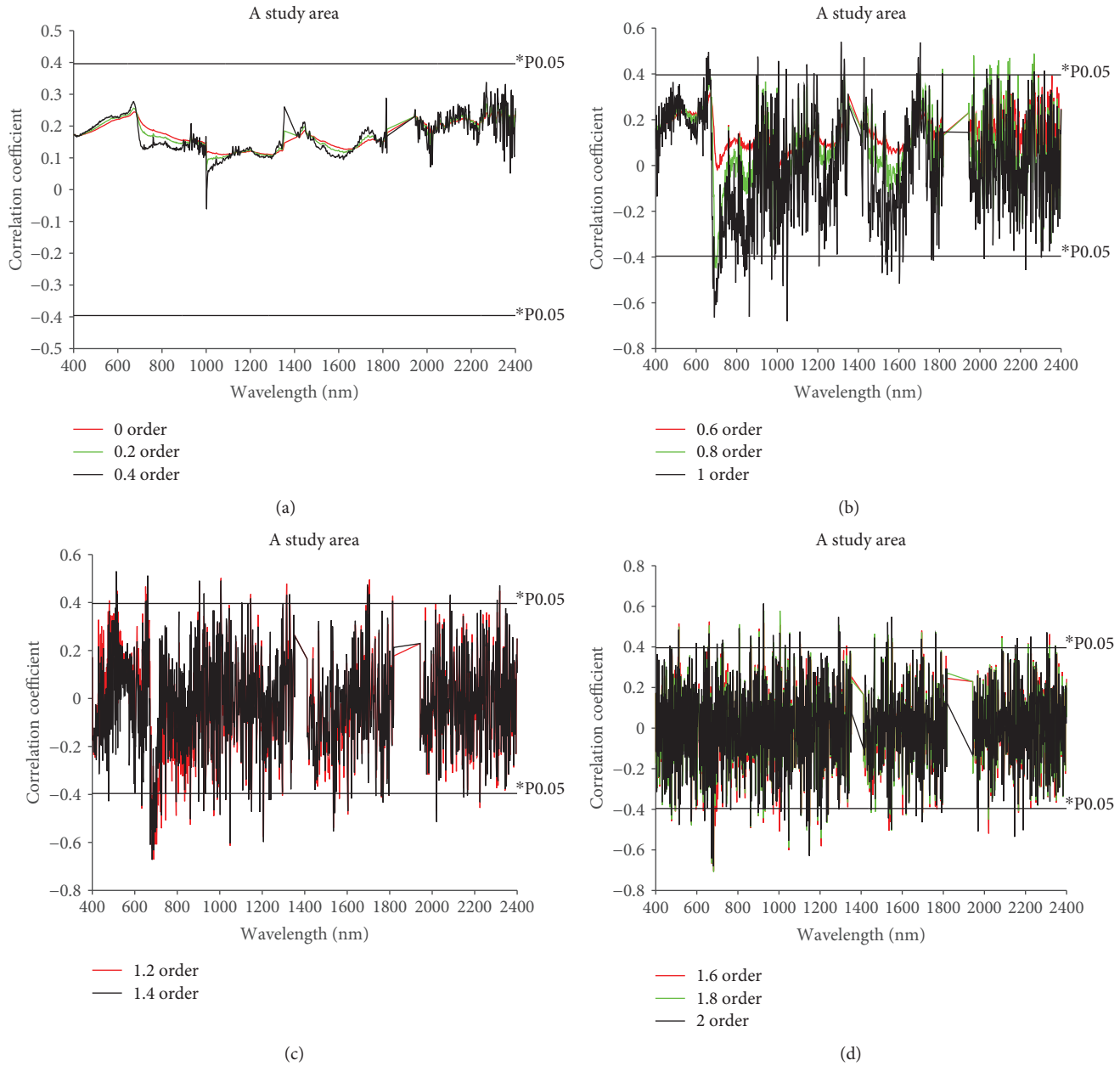

Figure 6: CC between salt content and raw spectral reflectance for area A. (a) 0–0.4-order differential. (b) 0.6–1st-order differential. (c) 1.2–1.4-order differential. (d) 1.6–2nd-order differential.

slowly moved towards the 1st-order differential curve. The difference between 1st-order and 2nd-differential values was very small. But the change trend still showed that in the process from 1st order to 2nd order, the differential curve slowly moved towards the 2nd-order differential curve. This verified that FD was sensitive and that FD calculation could render small differences between spectra under different human interference levels.

4.3. Effect of FD on the Correlation for the Full-Band Spectrum. Before quantitative analysis is conducted on the spectrum features of saline soil under different human interferences, we should first study the correlation between spectra and salt content and find the sensitive bands, which can increase the accuracy of the inversion model. In this study, we used raw spectral reflectance (R) as an example. Spectral reflectance was processed with MATLAB R2015 software using 0.2 as the order interval to analyze the correlation between salt content and R's 11-order differential (from 0 to 2nd order). The 0.05 test was used to determine the significance level. The $*$P0.05 for area A and area B was equal to plus or minus 0.396 and 0.361, respectively. Simulation result was shown in Figures 6 and 7.

When area A's raw spectral reflectance was between 0 and 0.5 orders, no band passed the 0.05 significance test. However, starting from 0.6 order, the bands passed the 0.05 significance test. Raw spectral reflectance bands in area B passed the 0.05 significance test starting from 0 order.

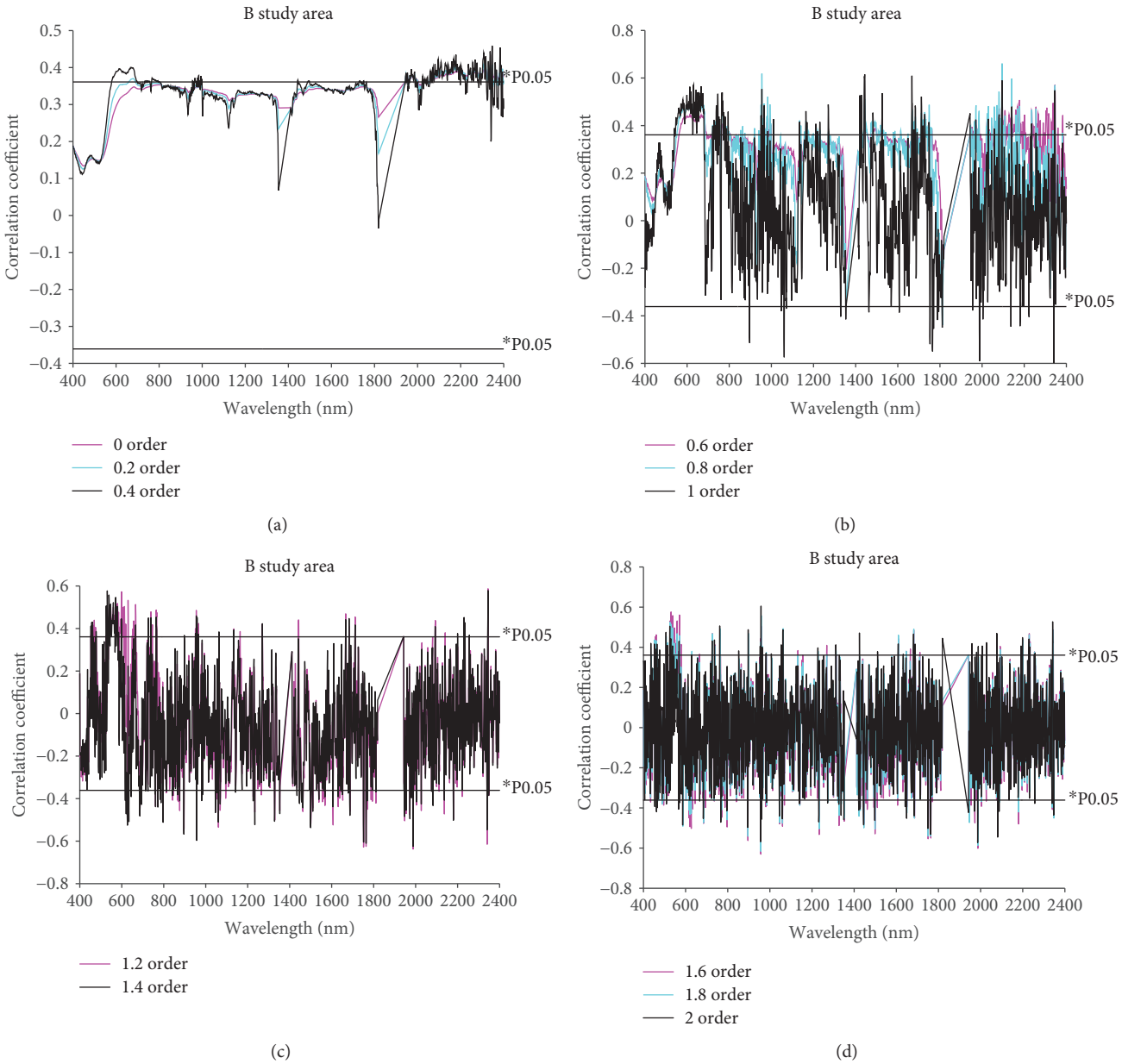

Figure 7: CC between salt content and raw spectral reflectance for area B. (a) 0–0.4-order differential. (b) 0.6–1st-order differential. (c) 1.2–1.4-order differential. (d) 1.6–2nd order differential.

Simulation result showed that FD calculation refined the curve change trend and reduced the loss of differential information. From 0 order to 0.7 order, the CC curve gradually showed a gradual trend and the gradual trend between each order's differential curve was presented. From 0.8 order to 2nd order, the CC curve of a gradual trend became less obvious and the curve fluctuation became greater.

4.4. Number of Bands Passed the 0.05 Significance Test. From Figures 6 and 7, it could be seen that as the order increases, so did the number of bands from areas A and B that passed the 0.05 significance test. However, the specific number of increase still required further statistical analysis. Thus, the number of bands from different order differentials for the five spectrum transformations that passed the 0.05 significance test was shown in Figure 8.

In area with no human interference, the sequence of the number of bands that passed the 0.05 significance test was as follows (from high to low): $1/R > \mathrm{Lg}R > \sqrt{R} > R > 1/\mathrm{Lg}R$. In area with human interference, the sequence of the number of bands that passed the 0.05 significance test was as follows (from high to low): $1/\mathrm{Lg}R > R > \sqrt{R} > \mathrm{Lg}R > 1/R$. In addition, the trend of bands that passed the 0.05 significance test showed an increase first then decrease later.

4.5. Bands with the Largest CC Absolute Value. In the five spectrum transformations, there were corresponding band information to the largest CC absolute value of 11 orders,

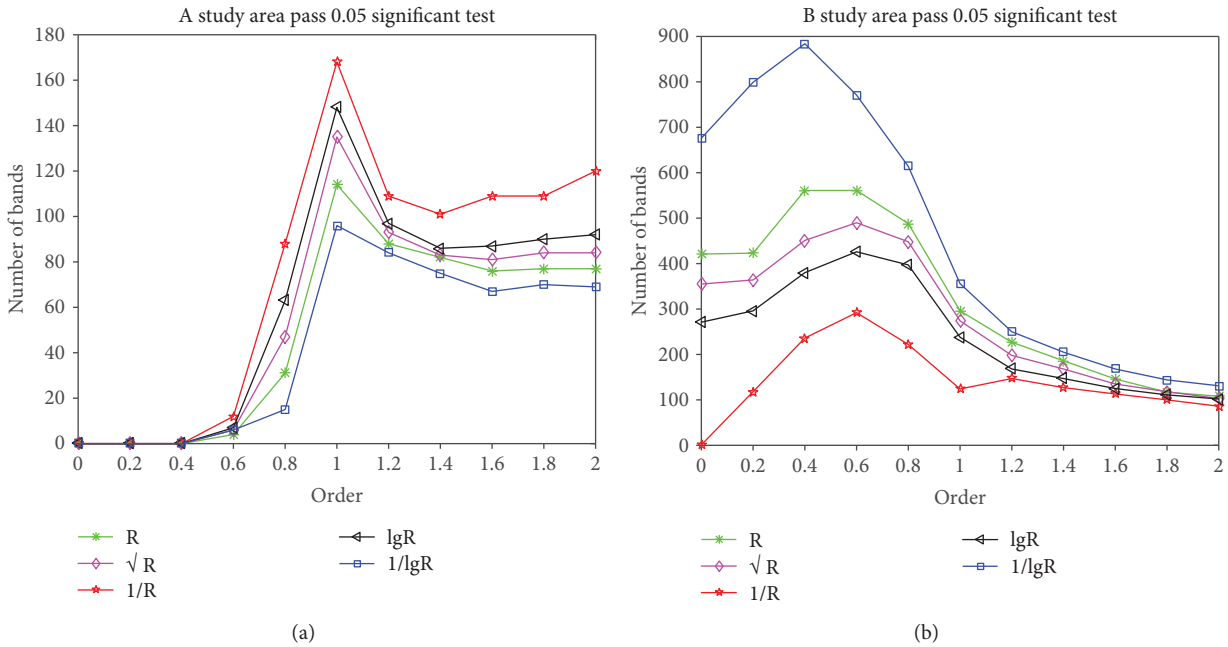

Figure 8: Number of bands passed the 0.05 significance test. (a) Area with no human interference. (b) Area with human interference.

Table 3: The bands with the largest CC absolute value in the no human interference area.

Order	R		$\sqrt{R}$		$1/R$ 676		LgR 676		$1/\mathrm{Lg}R$ 1946	
	Absolute	Band	Absolute	Band	Absolute	Band	Absolute	Band	Absolute	Band
0	0.247549	2355	0.258711	676	0.303965	676	0.273546	676	0.24171	1946
0.2	0.272918	2355	0.279275	2355	0.325149	672	0.289407	672	0.263505	2355
0.4	0.337521	2268	0.343669	2268	0.362546	2268	0.349886	2268	0.330819	2355
0.6	0.452251	2267	0.454245	2268	0.478337	2268	0.462786	2268	0.448415	2267
0.8	0.488129	2267	0.558134	693	0.651624	690	0.635344	693	0.487335	2267
1	0.680359	1049	0.694649	1049	0.693701	1049	0.700773	1049	0.649393	862
1.2	0.670618	689	0.674993	690	0.664982	690	0.678021	690	0.654813	689
1.4	0.672355	682	0.678587	682	0.666791	682	0.678755	682	0.656751	682
1.6	0.704214	682	0.70968	682	0.699427	682	0.710109	682	0.69164	682
1.8	0.708322	682	0.714082	682	0.709584	682	0.715906	682	0.697884	682
2	0.680375	681	0.686301	681	0.700033	1148	0.68948	681	0.671469	681

Table 4: The bands with the largest CC absolute value in the human interference area.

Order	R		$\sqrt{R}$		$1/R$ 676		LgR 676		$1/\mathrm{Lg}R$ 1946	
	Absolute	Band	Absolute	Band	Absolute	Band	Absolute	Band	Absolute	Band
0	0.39693	2384	0.390787	2384	0.361249	2384	0.382675	2384	0.407767	2310
0.2	0.41892	2384	0.412882	2384	0.384573	2383	0.405559	2383	0.4258	2384
0.4	0.45916	2346	0.456893	2383	0.457625	614	0.455213	2383	0.489956	2346
0.6	0.57097	2346	0.545842	2346	0.491625	668	0.515645	2346	0.608853	2346
0.8	0.66103	2095	0.640903	2095	0.593338	955	0.612877	955	0.67799	2095
1	0.61547	1443	0.615054	1988	0.598832	1988	0.625937	1988	0.64202	2095
1.2	0.63752	1988	0.64851	1988	0.631102	1764	0.652144	1988	0.629525	630
1.4	0.62432	1988	0.635681	1988	0.638534	1988	0.643132	1988	0.62093	531
1.6	0.63035	957	0.621285	957	0.589642	1987	0.610791	1987	0.64168	957
1.8	0.61592	957	0.605922	957	0.563155	957	0.593538	957	0.630378	957
2	0.60516	958	0.595053	958	0.553827	958	0.582938	958	0.621153	958

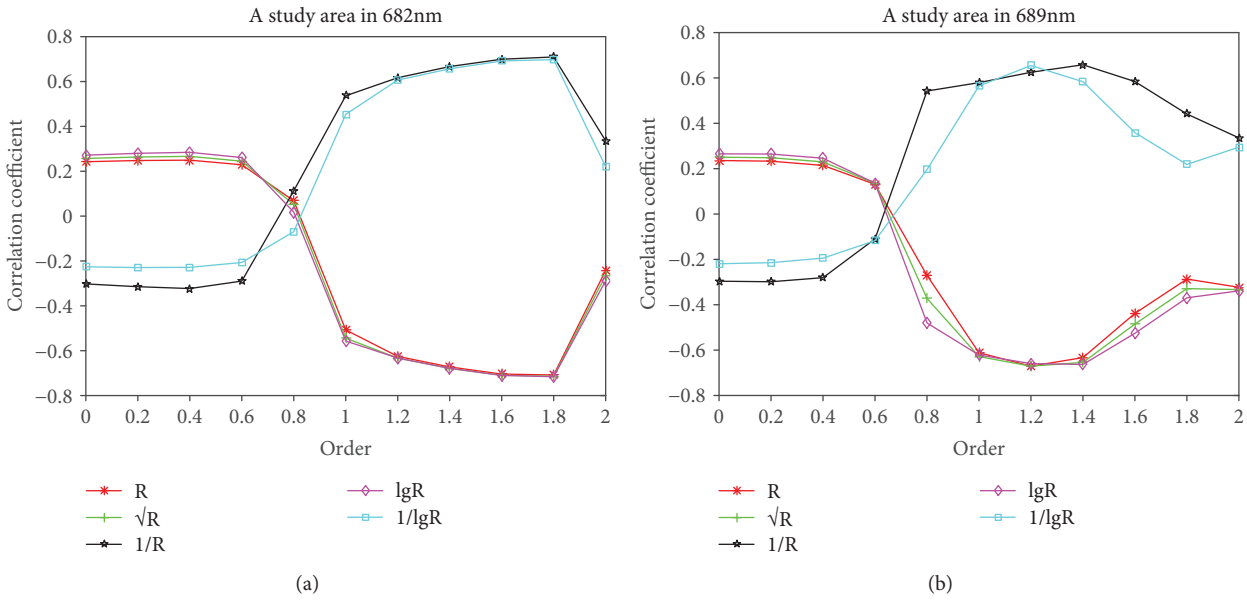

Figure 9: Changes in CC for area A. (a) 682 nm. (b) 689 nm.

as shown in Tables 3 and 4. In area A, the corresponding bands of the largest CC absolute value from various order differentials in the five transformations were in the 682 nm and they were all at 1.8 order. Also, the corresponding bands were in the 2095 nm and 1998 nm for area B, and they were located at 0.8 order or 1.2 order or 1.4 order.

Moreover, in the no human interference area, the largest CC of R is 0.708322, which was raised to the maximum CC of 0.715906 after LgR transformation at 1.8 order. Also, in the human interference area, R's biggest CC was 0.66103, it was promoted to the maximum CC of 0.67799 after 1/LgR transformation at 0.8 order. Statistical results showed that the largest CC from the five spectrum transformations in the no human interference area and human interference area appeared in the fractional order.

In addition, because the area A was affected by human activities, the soil characteristics were more complicated, so the maximum CC for area A was greater than area B. Moreover, the maximum CC absolute value was greater than 0.6, thus verified that the spectral reflectance and salt content were moderately related, close to the height correlation especially for area A, indicating that our research was valuable and the salt content could be predicted by spectra. So, we can use the pretreatment method for fractional differential to further verify the model in subsequent studies.

4.6. Impact of FD on the Correlation for Some Single-Band Spectrum. To further clarify the effect of FD calculation on some band's correlation, we chose the four bands in Tables 3 and 4 for our study on changes in CC as fractional orders change. For area A, we chose 682 nm, and 689 nm. For area B, we chose 957 nm and 1988 nm, as shown in Figures 9 and 10. FD calculation processing of the five spectral reflectance transformations significantly increased the absolute value of the CC; the maximum CC all appeared in the fractional order, and it was not in the integer differential (such as 1st or 2nd order) as in traditional analysis methods. We used 682 nm and 957 nm as examples to discuss the single-band correlation.

Figure 9(a) showed that the maximum CC absolute value of 682 nm for R, $\sqrt{R}$, 1/R, LgR, and 1/LgR was 0.70832, 0.71408, 0.70958, 0.71591, and 0.6978, respectively, which were at 1.8 order. Compared with 1st order, the maximum CC absolute value of five transformations were increased by 0.20091, 0.17003, 0.17307, 0.15902, and 0.24417, respectively. And they were improved by 0.46656, 0.44956, 0.37373, 0.42777, and 0.47757, respectively, when compared with 2nd order. Among them, the 1.8-order 1/LgR transformation had the largest improvement compared with the traditional integer order 1st order or 2nd order.

Figure 10(a) revealed that the largest CC absolute value of 957 nm for R, $\sqrt{R}$, 1/R, LgR, and 1/LgR was 0.63035, 0.62128, 0.57891, 0.60951, and 0.64168, respectively, all located at 1.6 order. Compared with the first order, the largest CC absolute value of five transformations were increased by 0.32788, 0.29408, 0.20445, 0.26160, and 0.39874, respectively. Compared with the second order, they were improved by 0.51078, 0.50334, 0.48060, 0.49566, and 0.53342, respectively. Among them, the 1.6-order 1/LgR transformation had the biggest improvement compared with the traditional integer order 1st order or 2nd order.

Furthermore, from Figures 9 and 10, it could be seen that the maximum CC for area A was also greater than area B for some single-band spectrum; it was also caused by human activities in area B to influence the soil features.

The main reason for the aforementioned results is that FD is an extension of the integer differential concept. Integer differential is only one of the special cases. Those can be explained in two ways.

On the one hand, due to fractional differential's memory and nonlocality, integer differential is only related to the band reflectance within the differential window. Equation

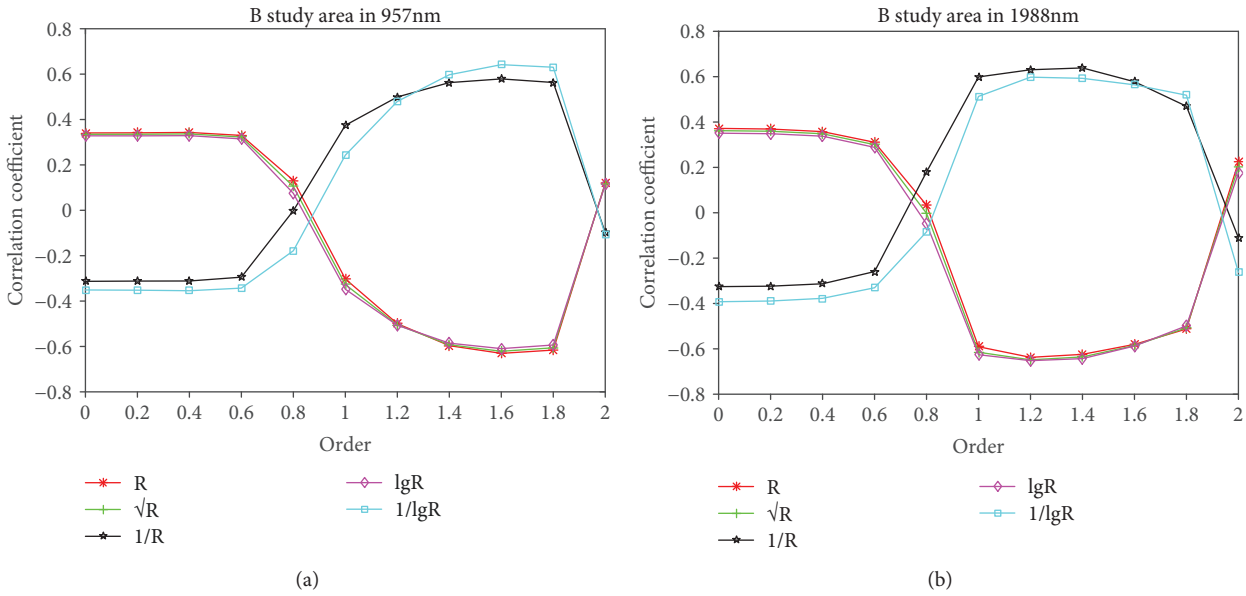

Figure 10: Changes in CC for area B. (a) 957 nm. (b) 1988 nm.

(3) shows that the FD value of certain bands is not only related to that band's reflectance but is also related to all the previous reflectance of that band [8]. Also, each point's reflectance is given a different weight according to the differential order. Greater weight is given to closer points. Thus, that band's FD impact is also greater. In addition, this is the one of the greatest difference between FD and integer differential.

On the other hand, some studies show that many systems belong to fractional order [8, 9, 29, 30], and we traditionally use the integer-order differential model for spectral processing; this leads to a greater difference between the model and actual results, and low accuracy of system simulation and prediction. As a result, this also neglects the system's realism.

5. Conclusion

In this study, we introduced FD into hyperspectral data pretreatment. Saline soil spectral reflectance data from field spectrum measurements taking in Xinjiang's Fukang City was adopted as a basis. FD processing was used on raw spectral reflectance and its common mathematical transformation to explore the effect of FD calculation on the CC between saline soil hyperspectral reflectance and soil salt content in fields with different levels of human interference. The main conclusion was that the soil properties of zone B were more complex than zone A, because zone B was affected by human activities. Under different human interference levels, FD calculation could describe small difference between spectra. The overall differential value trend was towards a reflectance value of 0. After differential processing, the number of bands that passed the 0.05 significance test first increased then decreased; the changes in trends were depicted through fractional differential. For different human interference areas, the largest CC absolute value of the five spectrum transformations all appeared in the fractional order. For full-band or some single bands (689 nm, 682 nm, 1988 nm, and 957 nm), the differential transformation could significantly increase the correlation between spectral reflectance and soil salt content. The extreme value could be obtained in the fractional order. Therefore, FD enriched the hyperspectral data pretreatment. We explored latent spectrum data information from a FD perspective and used hyperspectral data to provide a new perspective for field hyperspectral monitoring of soil salinization in areas with different levels of human interference.

Data Availability

The data used to support the findings of this study will be available from the corresponding author upon request after this project has been finished in 2021.

Conflicts of Interest

The authors declare that they have no conflict of interest.

Acknowledgments

This research was supported by the financial support of the National Natural Science Foundation of China (41761081, 41671198, and 41861054) and Yunnan Province Science and Technology Department and Education Department Project of China (2017FH001-067, 2017FH001-117, and 2016ZDX127).

References

[1] X. X. Qiao, C. Wang, M. C. Feng et al., "Hyperspectral estimation of soil organic matter based on different spectral preprocessing techniques," *Spectroscopy Letters*, vol. 50, no. 3, pp. 156–163, 2017.

[2] Y. M. Zheng, T. Q. Zhang, J. Zhang, X. D. Chen, and X. G. Shen, "Influence of smooth, 1st derivative and baseline correction on the near-infrared spectrum analysis with PLS,"

Spectroscopy and Spectral Analysis, vol. 24, no. 12, pp. 1546–1548, 2004.

[3] F. Zhang, J. L. Ding, Tashpolat, Tiyip, and Q. S. He, "Spectral data analysis of salinity soils with ground objects in the delta oasis of Weigan and Kuqa Rivers," *Spectroscopy and Spectral Analysis*, vol. 28, no. 12, pp. 2921–2926, 2008.

[4] J. Wang, J. Ding, A. Abulimiti, and L. Cai, "Quantitative estimation of soil salinity by means of different modeling methods and visible-near infrared (VIS-NIR) spectroscopy, Ebinur Lake Wetland, Northwest China," *PeerJ*, vol. 6, article e4703, 2018.

[5] J. M. Schmitt, "Fractional derivative analysis of diffuse reflectance spectra," *Applied Spectroscopy*, vol. 52, no. 6, pp. 840–846, 1998.

[6] S. S. Kharintsev and M. K. Salakhov, "A simple method to extract spectral parameters using fractional derivative spectrometry," *Spectrochimica Acta Part A: Molecular and Biomolecular Spectroscopy*, vol. 60, no. 8-9, pp. 2125–2133, 2004.

[7] K.-Y. Zheng, X. Zhang, P.-J. Tong, Y. Yao, and Y.-P. Du, "Pretreating near infrared spectra with fractional order Savitzky–Golay differentiation (FOSGD)," *Chinese Chemical Letters*, vol. 26, no. 3, pp. 293–296, 2015.

[8] Z. Dong, T. Tiyip, Z. Fei, and A. Kelimu, "Application of fractional differential in preprocessing hyperspectral data of saline soil," *Transactions of the Chinese Society of Agricultural Engineering*, vol. 30, no. 24, pp. 151–160, 2014.

[9] N. Xia, T. Tiyip, A. Kelimu et al., "Influence of fractional differential on correlation coefficient between $EC_{1:5}$ and reflectance spectra of saline soil," *Journal of Spectroscopy*, vol. 2017, Article ID 1236329, 11 pages, 2017.

[10] P. C. Duan, H. G. Xiong, R. R. Li, and L. Zhang, "A quantitative analysis of the reflectance of the saline soil under different disturbance extent," *Spectroscopy and Spectral Analysis*, vol. 37, no. 2, pp. 571–576, 2017.

[11] C. R. Bern, M. L. Clark, T. S. Schmidt, J. A. M. Holloway, and R. R. Mcdougal, "Soil disturbance as a driver of increased stream salinity in a semiarid watershed undergoing energy development," *Journal of Hydrology*, vol. 524, pp. 123–136, 2015.

[12] H. Triki Fourati, M. Bouaziz, M. Benzina, and S. Bouaziz, "Modeling of soil salinity within a semi-arid region using spectral analysis," *Arabian Journal of Geosciences*, vol. 8, no. 12, pp. 11175–11182, 2015.

[13] M. Elhag, "Evaluation of different soil salinity mapping using remote sensing techniques in arid ecosystems, Saudi Arabia," *Journal of Sensors*, vol. 2016, Article ID 7596175, 8 pages, 2016.

[14] A. Abbas, S. Khan, N. Hussain, M. A. Hanjra, and S. Akbar, "Characterizing soil salinity in irrigated agriculture using a remote sensing approach," *Physics and Chemistry of the Earth, Parts A/B/C*, vol. 55-57, pp. 43–52, 2013.

[15] J. Ding and D. Yu, "Monitoring and evaluating spatial variability of soil salinity in dry and wet seasons in the Werigan–Kuqa Oasis, China, using remote sensing and electromagnetic induction instruments," *Geoderma*, vol. 235-236, pp. 316–322, 2014.

[16] Z. Miao and W. Shi, "A new methodology for spectral-spatial classification of hyperspectral images," *Journal of Sensors*, vol. 2016, Article ID 1538973, 12 pages, 2016.

[17] T. Shi, L. Cui, J. Wang, T. Fei, Y. Chen, and G. Wu, "Comparison of multivariate methods for estimating soil total nitrogen with visible/near-infrared spectroscopy," *Plant and Soil*, vol. 366, no. 1-2, pp. 363–375, 2013.

[18] P. Pornchaloempong, P. Sirisomboon, and S. Pongkuan, "Rapid evaluation of the salt content of canned sardines in brine using near-infrared diffuse reflectance spectroscopy," *Spectroscopy Letters*, vol. 49, no. 10, pp. 613–618, 2016.

[19] J. L. Ding, Y. Yao, and F. Wang, "Detecting soil salinization in arid regions using spectral feature space derived from remote sensing data," *Acta Ecologica Sinica*, vol. 34, no. 16, 2014.

[20] S. Chen, X. Bin, Y. X. Jin et al., "Remote sensing monitoring and spatial-temporal features analysis of soil salinization in agricultural area of Northern Xinjiang," *Scientia Geographica Sinica*, vol. 35, no. 12, pp. 1607–1615, 2015.

[21] D. An, G. Zhao, C. Chang et al., "Hyperspectral field estimation and remote-sensing inversion of salt content in coastal saline soils of the Yellow River Delta," *International Journal of Remote Sensing*, vol. 37, no. 2, pp. 455–470, 2016.

[22] R. Sahadevan and P. Prakash, "Exact solutions and maximal dimension of invariant subspaces of time fractional coupled nonlinear partial differential equations," *Communications in Nonlinear Science and Numerical Simulation*, vol. 42, pp. 158–177, 2017.

[23] B. Safarinejadian, M. Asad, and M. S. Sadeghi, "Simultaneous state estimation and parameter identification in linear fractional order systems using coloured measurement noise," *International Journal of Control*, vol. 89, no. 11, pp. 2277–2296, 2016.

[24] S. M. Shah, R. Samar, N. M. Khan, and M. A. Z. Raja, "Fractional-order adaptive signal processing strategies for active noise control systems," *Nonlinear Dynamics*, vol. 85, no. 3, pp. 1363–1376, 2016.

[25] A. C. Iznaga, M. R. Orozco, E. A. Alcantara et al., "Vis/NIR spectroscopic measurement of selected soil fertility parameters of Cuban agricultural Cambisols," *Biosystems Engineering*, vol. 125, no. 125, pp. 105–121, 2014.

[26] F. Zhang, T. Tiyip, J. Ding et al., "Studies on the reflectance spectral features of saline soil along the middle reaches of Tarim River: a case study in Xinjiang Autonomous Region, China," *Environmental Earth Sciences*, vol. 69, no. 8, pp. 2743–2761, 2013.

[27] M. C. Sarathjith, B. S. Das, S. P. Wani, and K. L. Sahrawat, "Dependency measures for assessing the covariation of spectrally active and inactive soil properties in diffuse reflectance spectroscopy," *Soil Science Society of America Journal*, vol. 78, no. 5, 2014.

[28] Z. Dong, *Application Research of Fractional Derivative on the Remote Sensing Monitoring of Soil Salinization [D]*, Xinjiang University, Urumqi, 2017.

[29] T. J. Freeborn, B. Maundy, and A. S. Elwakil, "Measurement of supercapacitor fractional-order model parameters from voltage-excited step response," *IEEE Journal on Emerging and Selected Topics in Circuits and Systems*, vol. 3, no. 3, pp. 367–376, 2013.

[30] G. S. M. Ngueuteu and P. Woafo, "Dynamics and synchronization analysis of coupled fractional-order nonlinear electromechanical systems," *Mechanics Research Communications*, vol. 46, pp. 20–25, 2012.